AN204470

FM3 Family, Position Estimation of PMSM with Signal Injection

This application note describes HFI-based observer for salient PMSM, including zero speed position estimation, polarity detection, and low speed position estimation.

Contents

1 Introduction

1.1 Purpose

The function of widely-applied EMF position observer is limited for there is no EMF at zero speed or the EMF is small at low speed. This document describes HFI-based observer for salient PMSM, including zero speed position estimation, polarity detection, and low speed position estimation.

1.2 Definitions, Acronyms and Abbreviations

HFI	High Frequency signal Injection
LPF	Low Pass Filter
BPF	Band Pass Filter
PWM	Pulse Width Modulation
PLL	Phase Lock Loop

1.3 Document Overview

The rest of document is organized as the following:

Chapter 2 explains Position Estimation through HFI at Zero Speed.

Chapter 3 explains Polarity Detection with Knowledge of d-axis Alignment.

Chapter 4 explains Position Estimation through HFI at Low Speed.

Chapter 5 explains *Experiment Result.*

2 Position Estimation through HFI at Zero Speed

2.1 Fundamental of HFI-Based Position Estimation

2.1.1 PMSM Model

The PMSM modeled in stationary reference frame is

$$\begin{bmatrix} V_\alpha \\ V_\beta \end{bmatrix} = R_s \begin{bmatrix} i_\alpha \\ i_\beta \end{bmatrix} + \frac{d}{dt} \begin{bmatrix} L_\alpha & L_{\alpha\beta} \\ L_{\alpha\beta} & L_\beta \end{bmatrix} \begin{bmatrix} i_\alpha \\ i_\beta \end{bmatrix} + \lambda_f \omega_r \begin{bmatrix} -sin\theta \\ cos\theta \end{bmatrix} \quad (2\text{-}1)$$

where the ideal model of induction matrix is

$$\begin{bmatrix} L_\alpha & L_{\alpha\beta} \\ L_{\alpha\beta} & L_\beta \end{bmatrix} = \begin{bmatrix} L_0 + L_1 cos2\theta & L_1 sin2\theta \\ L_1 sin2\theta & L_0 - L_1 cos2\theta \end{bmatrix} \quad (2\text{-}2)$$

When PMSM is under standstill case ($\theta = constant, \omega_r = 0$), motor model is simplified as

$$\begin{bmatrix} V_\alpha \\ V_\beta \end{bmatrix} = R_s \begin{bmatrix} i_\alpha \\ i_\beta \end{bmatrix} + \begin{bmatrix} L_\alpha & L_{\alpha\beta} \\ L_{\alpha\beta} & L_\beta \end{bmatrix} \frac{d}{dt} \begin{bmatrix} i_\alpha \\ i_\beta \end{bmatrix} \quad (2\text{-}3)$$

Further investigating high frequency signal response of motor, and ignore resistance (assuming $R_s \ll 2\pi f_{hf} L_*$), current response to injected high frequency voltage is

$$\begin{bmatrix} i_\alpha \\ i_\beta \end{bmatrix} = \begin{bmatrix} L_\alpha & L_{\alpha\beta} \\ L_{\alpha\beta} & L_\beta \end{bmatrix}^{-1} \int \begin{bmatrix} V_\alpha \\ V_\beta \end{bmatrix} dt = \frac{1}{L_0^2 - L_1^2} \begin{bmatrix} L_0 - L_1 cos2\theta & -L_1 sin2\theta \\ -L_1 sin2\theta & L_0 + L_1 cos2\theta \end{bmatrix} \begin{bmatrix} \lambda_\alpha \\ \lambda_\beta \end{bmatrix} \quad (2\text{-}4)$$

$$\begin{bmatrix} \lambda_\alpha \\ \lambda_\beta \end{bmatrix} = \int \begin{bmatrix} V_\alpha \\ V_\beta \end{bmatrix} dt \quad (2\text{-}5)$$

Apply park transformation

$$\begin{bmatrix} i_d \\ i_q \end{bmatrix} = \frac{1}{L_0^2 - L_1^2} \begin{bmatrix} L_q & 0 \\ 0 & L_d \end{bmatrix} \begin{bmatrix} \lambda_d \\ \lambda_q \end{bmatrix} \quad (2\text{-}6)$$

Similarly, transform stationary model into estimated rotating reference frame with $\hat{\theta}$

$$\begin{bmatrix} i_{dc} \\ i_{qc} \end{bmatrix} = \frac{1}{L_0^2 - L_1^2} \begin{bmatrix} L_0 - L_1 cos2\tilde{\theta} & -L_1 sin2\tilde{\theta} \\ -L_1 sin2\tilde{\theta} & L_0 + L_1 cos2\tilde{\theta} \end{bmatrix} \begin{bmatrix} \lambda_{dc} \\ \lambda_{qc} \end{bmatrix} \quad (2\text{-}7)$$

2.1.2 Initial Position Estimation with Pulsating High Frequency Voltage Injection

Injecting high frequency voltage on estimated rotating reference frame such that

$$\begin{bmatrix} V_{dc} \\ V_{qc} \end{bmatrix} = V_h \begin{bmatrix} cos\omega_{hf} t \\ 0 \end{bmatrix} \quad (2\text{-}8)$$

where V_{hf} and ω_{hf} are magnitude and frequency of high frequency voltage, respectively. Therefore, flux linkage is

$$\begin{bmatrix} \lambda_{dc} \\ \lambda_{qc} \end{bmatrix} = \frac{V_{hf}}{\omega_{hf}} \begin{bmatrix} sin\omega_{hf} t \\ 0 \end{bmatrix} \quad (2\text{-}9)$$

And current response is

$$\begin{bmatrix} i_{dc} \\ i_{qc} \end{bmatrix} = \frac{V_{hf}}{\omega_{hf}} \frac{1}{L_0^2 - L_1^2} \begin{bmatrix} L_0 - L_1 cos2\tilde{\theta} \\ -L_1 sin2\tilde{\theta} \end{bmatrix} sin\omega_{hf} t \quad (2\text{-}10)$$

Apparently, i_{qc} contains position error information, and rotor position is observable at zero speed. Particularly, i_{qc} is modulated with $2sin\omega_{hf} t$ and filtered by a low pass filter and remaining signal is

$$LPF\left(i_{qc} * 2 * sin\omega_{hf} t\right) = LPF\left(-\frac{V_{hf}}{\omega_{hf}} \frac{L_1}{L_0^2 - L_1^2} sin2\tilde{\theta}\left(1 - cos2\omega_{hf} t\right)\right) \approx -\frac{V_{hf}}{\omega_{hf}} \frac{L_1}{L_0^2 - L_1^2} sin2\tilde{\theta}$$

2.2 HFI Implementation

Figure 1. Block Diagram of HFI Based Position Estimation

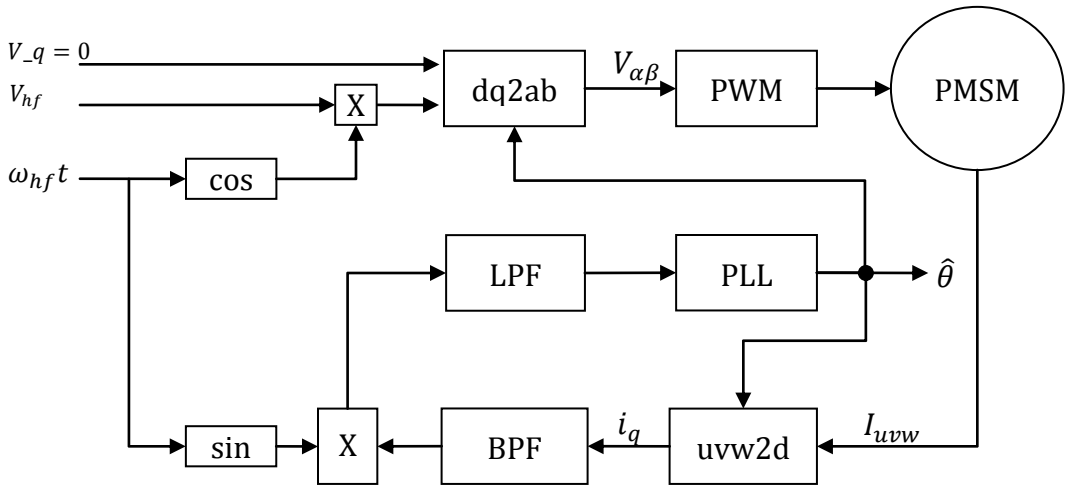

Figure 1 shows the block diagram of HFI based position estimation scheme. Two main blocks are included:

1. High frequency signal generating block
2. Position estimation block
3. The position estimation block processes current signal, extracted high frequency response, and estimates rotor position.
4. Band pass filter:
5. A second order band pass filter is implemented into HFI block. Although only high frequency voltage is injected (no fundamental excitation), sampled stator current contains required high frequency current as well as noise due to nonlinearity of PWM, DC bus harmonics, etc. Therefore, a BPF is preferred to eliminate the unwanted noise.
6. Low Pass Filter
7. The modulated current includes a high frequency signal with twice frequency of injected signal. Whether the LPF is needed depends on PLL algorithm, since a PLL algorithm has a limited band pass that suppresses this high frequency signal.
8. Phase Lock Loop
9. The PLL algorithm is designed to estimate rotor position. Figure 2 shows the block diagram of a general PLL. With transfer function as

$$\frac{\theta}{\tilde{\theta}} = \frac{K_P s + K_I}{s^2 + K_P s + K_I} \tag{2-11}$$

In standstill case, an integration regulator may lead to instable position output. Thus only a P-regulator is implemented (with $K_I = 0$).

Figure 2. General PLL Block Diagram

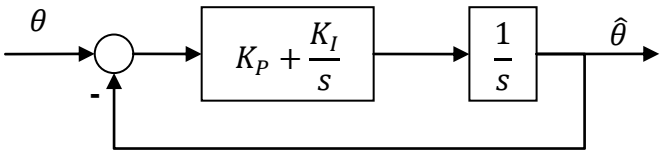

Note: The current response to high frequency voltage shows that PLL forces i_{qc} to zero, which means $sin2\tilde{\theta} \rightarrow 0$, and 2 equilibrium points can be obtained:

$$\begin{cases}\tilde{\theta} = 0 \\ \tilde{\theta} = \pi\end{cases} \tag{2-12}$$

Therefore, polarity detection is required to identify the convergence point of HFI.

3 Polarity Detection with Knowledge of d-axis Alignment

The HFI-based position estimation function estimates rotor position according to the saliency property of PMSM. However, ambiguous d-axis position requires a further polarity detection scheme to correct initial position.

3.1 Fundamental of Polarity Detection

The saturation-caused nonlinearity of inductance is the basis of polarity detection. According to Tyler series, d-axis inductance is approximated as

$$L_d(i_d) \approx L_d(i_d = 0) + \frac{\partial L_d(i_d)}{\partial i_d} i_d + \frac{\partial^2 L_d(i_d)}{\partial i_d^2} i_d^2 + O^2(0) \tag{3-1}$$

Figure 3. Nonlinearity of L_d as function of i_d

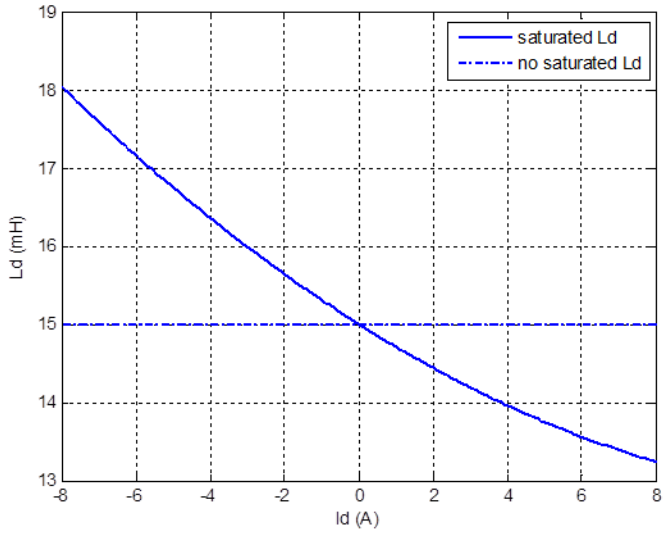

In terms of above approximation, two categories of polarity detection are widely investigated:

1. First order approximation based polarity detection
2. Second order approximation based polarity detection

In this document, the first order approximation based polarity detection is adopted due to small amplitude of second order approximation.

Assuming zero condition with constant L_d, current response to voltage step aligns on d-axis is

$$i_d(t) = \frac{V_d}{R_s}(1 - e^{-\frac{R_s}{L_d}t}) \tag{3-2}$$

Current attenuation process with constant L_d is

$$i_d(t) = i_d(0)e^{-\frac{R_s}{L_d}t} \tag{3-3}$$

Therefore, current response to voltage pulse is theoretically obtained. Figure 4 shows the simulation result of current response to a first order approximated inductance.

Figure 4. d-axis current response to voltage pulse

Blue: constant inductance, Pink: first order approximated inductance

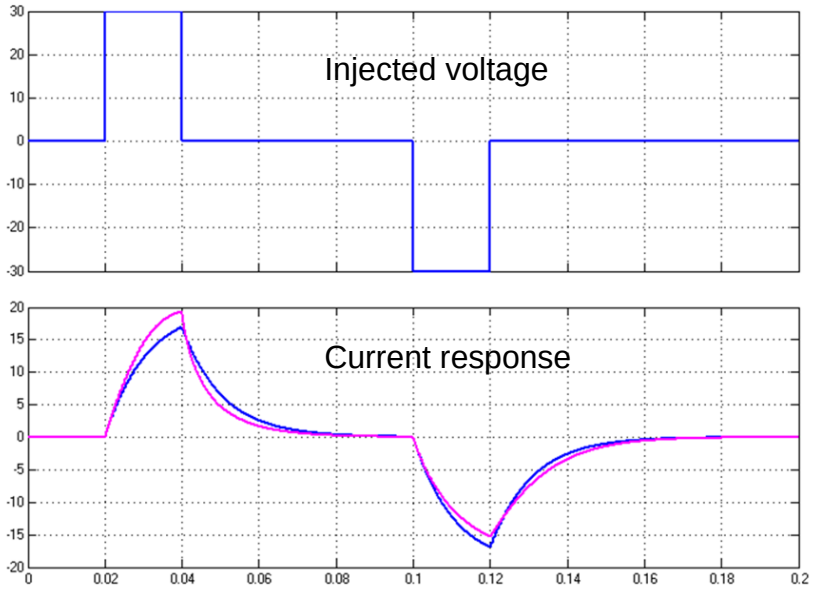

Analytical result is thus summarized as below

1. Charging process

$$\left|I_{peak}(V_d = V_s)\right| > \left|I_{peak}(V_d = -V_s)\right| \tag{3-4}$$

Note: Above equation is ONLY effective under transient current response, since stationary amplitudes are the same because (Figure 6).

$$\lim_{t\to\infty} \frac{V_d}{R_s}\left(1 - e^{-\frac{R_s}{L_d}t}\right) = \frac{V_d}{R_s} \tag{3-5}$$

2. Discharging process

Current propagation in a sample interval is (L_d is assumed constant in such a short time interval)

$$i_d(n+1) = i_d(n)e^{-\frac{R_s}{L_d}T_s} = Ki_d(n) \tag{3-6}$$

Therefore, the gradient can be estimated to identify polarity:

$$\boldsymbol{K}(i_d > 0) < \boldsymbol{K}(i_d < 0) \tag{3-7}$$

3.2 Polarity Detection through Peak Current

3.2.1 Process

Figure 5. Flow Chart of Current Peak-Based Polarity Detection

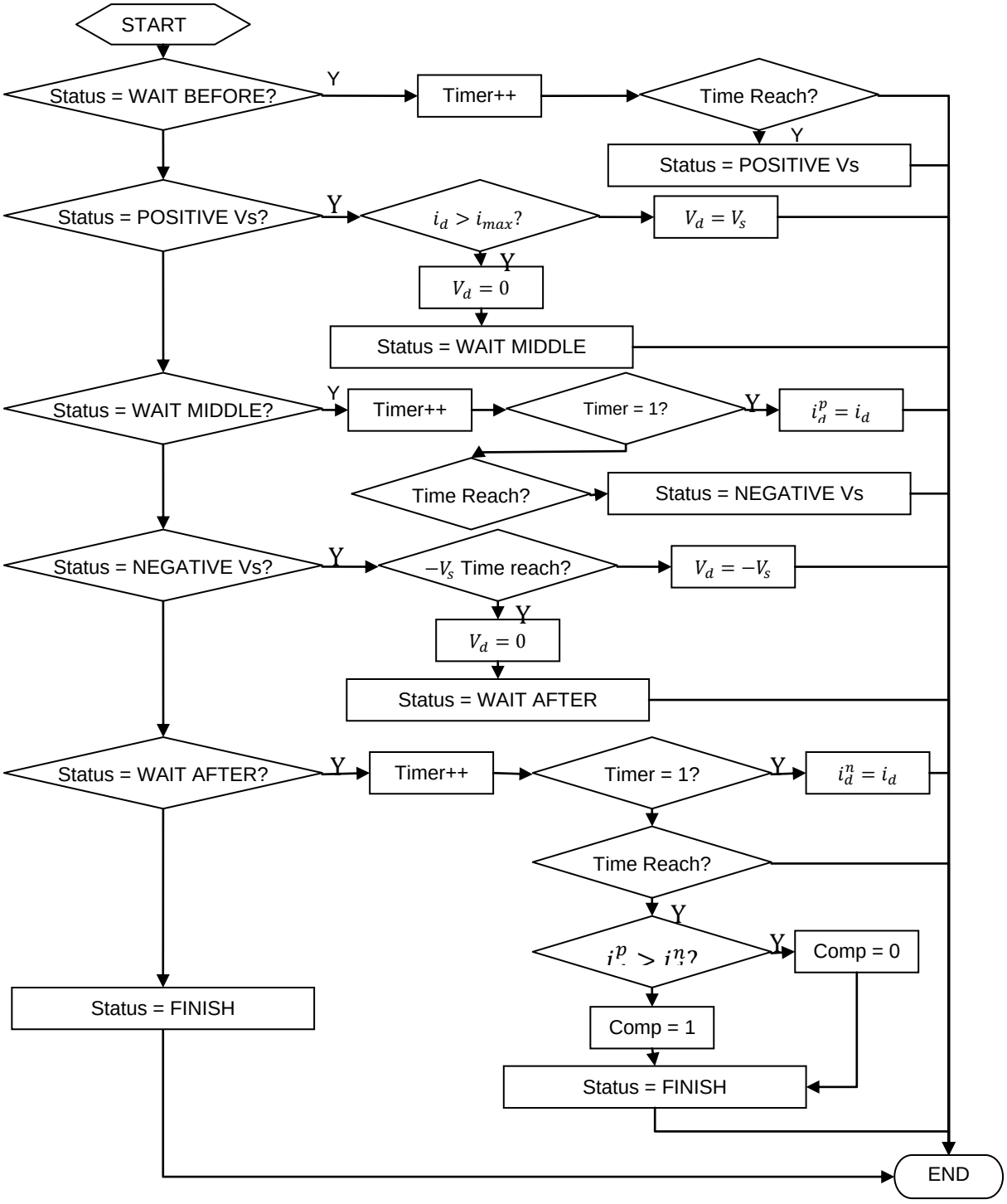

3.2.2 Implementation Issues

Figure 6 shows current difference between positive and negative voltage injection. A maximum difference point is preferred since it tells polarity obviously. However, the numerical solution of this point is difficult to predict in MCU. Parameter setup should consider sample resolution and signal-to-noise ratio, electrical constant of motor, sample frequency, etc.

Noise in sample usually appears (ignore bias) in control system, and one peak sample may deviate from actual value in noisy case and lead to detection failure. Therefore sampling and processing multiple points is a better choice to counteract this drawback.

Current attenuation in the neighborhood of peak current is

$$i_d(t) = i_d(0)e^{-\frac{R_s}{L_d}t} \tag{3-8}$$

And current variation in short time interval is approximated as

$$\frac{\Delta i_d}{i_d(0)} = \frac{\partial i_d}{\partial t}\frac{\Delta t}{i_d(0)} = -\frac{\Delta t}{L_d/R_s} \tag{3-9}$$

Therefore, if sample time satisfies$T_s \ll L_d/R_s$, the neighborhood of peak current can be sampled to assist peak current identification.

Figure 6. Current response to positive and negative voltage pulse and their difference

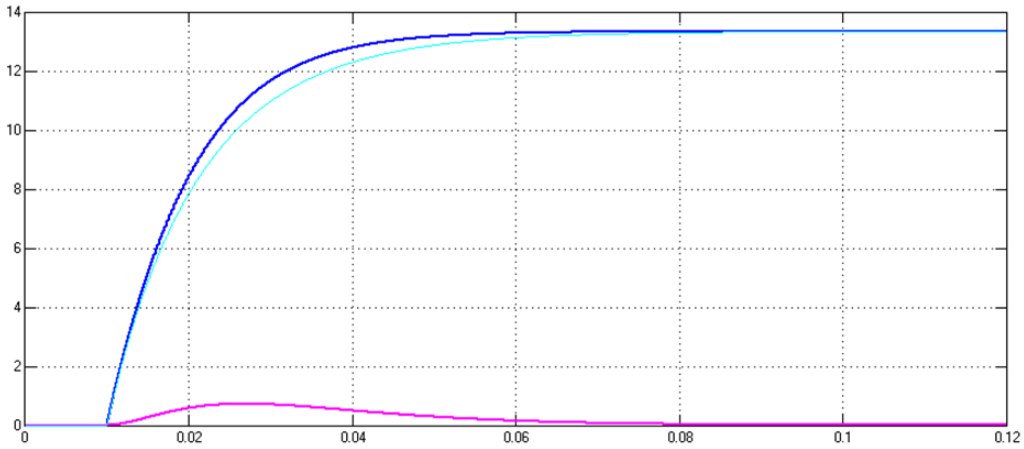

3.3 Polarity Detection through Current Attenuation

3.3.1 Process

Figure 7 shows the flow chart of current attenuation-based polarity detection. Current attenuation detection is realized through least square estimation. Consider following linear model

$$y(n) = Kx(n) \tag{3-10}$$

The best estimation by means of least square is

$$\widehat{K}(N) = \frac{\sum_{n=1}^{N} x(n)y(n)}{\sum_{n=1}^{N} x^2(n)} \tag{3-11}$$

Define

$$y(n) = i_d(n+1) \tag{3-12}$$

$$x(n) = i_d(n) \tag{3-13}$$

$$K = e^{-\frac{R_s}{L_d}T_s} \tag{3-14}$$

K is thus estimated and polarity detection is done by estimating $K(i_d > 0)$ and $K(i_d < 0)$, respectively.

Figure 7. Flow Chart of Current Attenuation Based Polarity Detection

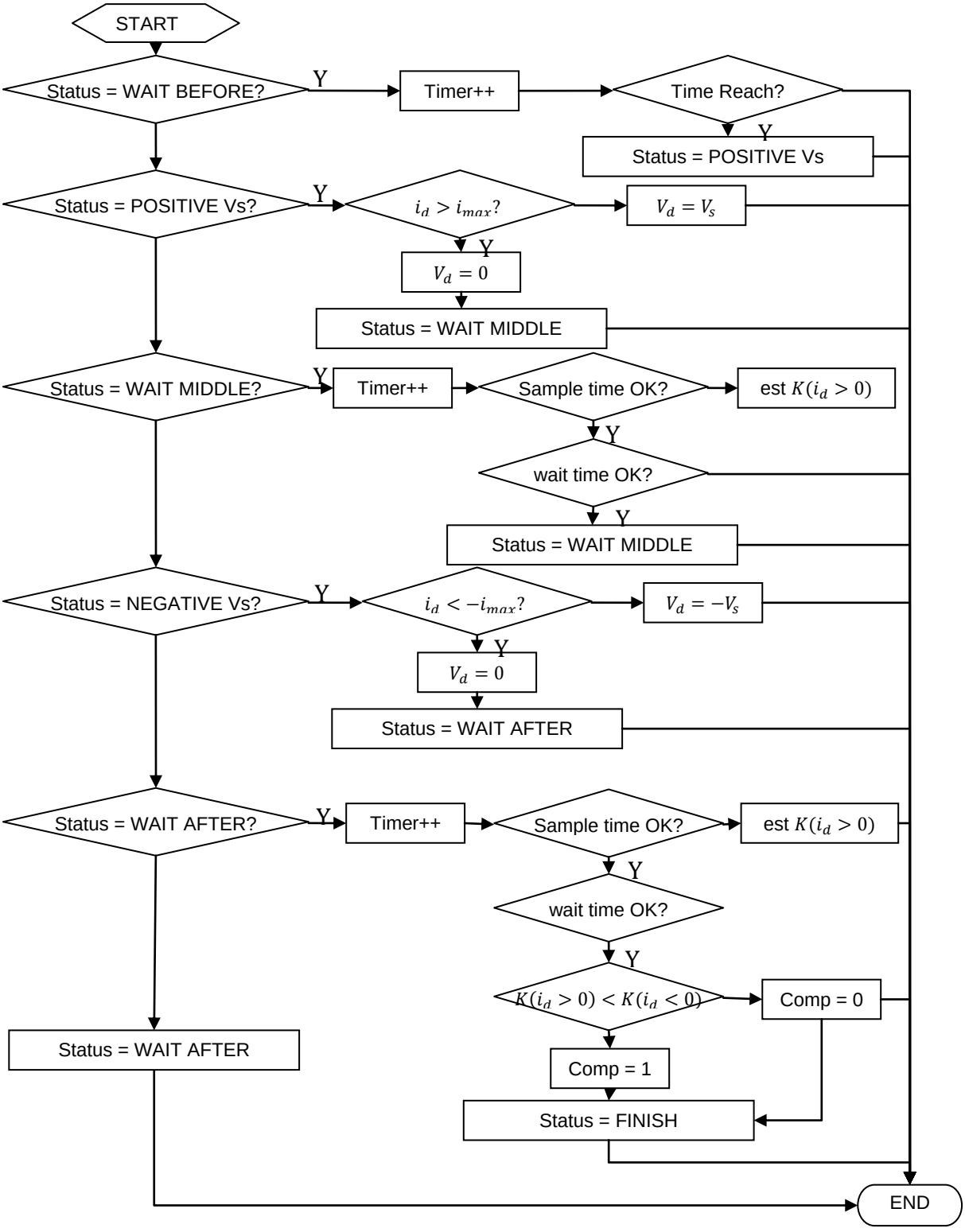

4 Position Estimation through HFI at Low Speed

4.1 PMSM Model and High Frequency Voltage Response at Low Speed

PMSM model in estimated reference frame with non-zero speed is expressed as

$$\begin{bmatrix} V_{dc} \\ V_{qc} \end{bmatrix} = \frac{d}{dt}\begin{bmatrix} \lambda_{dc} \\ \lambda_{qc} \end{bmatrix} + \hat{\omega} J \begin{bmatrix} \lambda_{dc} \\ \lambda_{qc} \end{bmatrix} \quad (4\text{-}1)$$

where

$$\begin{bmatrix} \lambda_{dc} \\ \lambda_{qc} \end{bmatrix} = \mathbb{L}_{dqc}\begin{bmatrix} i_{dc} \\ i_{qc} \end{bmatrix} + \lambda_f \begin{bmatrix} cos\tilde{\theta} \\ sin\tilde{\theta} \end{bmatrix} \quad (4\text{-}2)$$

And inductance matrix is

$$\mathbb{L}_{dqc} = \begin{bmatrix} L_0 + L_1 cos2\tilde{\theta} & L_1 sin2\tilde{\theta} \\ L_1 sin2\tilde{\theta} & L_0 - L_1 cos2\tilde{\theta} \end{bmatrix} + \begin{bmatrix} -L_{dq} sin2\tilde{\theta} & L_{dq} cos2\tilde{\theta} \\ L_{dq} cos2\tilde{\theta} & L_{dq} sin2\tilde{\theta} \end{bmatrix} + \begin{bmatrix} L_2\, cos\left(h_2\theta + 2\tilde{\theta}\right) & L_2\, sin\left(h_2\theta + 2\tilde{\theta}\right) \\ L_2\, sin\left(h_2\theta + 2\tilde{\theta}\right) & -L_2\, cos\left(h_2\theta + 2\tilde{\theta}\right) \end{bmatrix} \quad (4\text{-}3)$$

In which L_{dq} is cross coupling inductance, L_2 and h_2 are magnitude and order of the secondary salience. Equation (4-3) modeled the nonlinearity of cross coupling and secondary salience.

Let stator flux linkage distributed as

$$\begin{bmatrix} \lambda_{dch} \\ \lambda_{qch} \end{bmatrix} = \frac{V_{hf}}{\omega_{hf}}\begin{bmatrix} sin\omega_{hf}t \\ 0 \end{bmatrix} \quad (4\text{-}4)$$

The injected high frequency voltage should be

$$\begin{bmatrix} V_{dc} \\ V_{qc} \end{bmatrix} = V_{hf}\begin{bmatrix} cos\omega_{hf}t \\ \frac{\hat{\omega}}{\omega_{hf}} sin\omega_{hf}t \end{bmatrix} \quad (4\text{-}5)$$

And the high frequency current response is

$$i_{dc} = \frac{V_{hf}}{\omega_{hf}\|\mathbb{L}_{dqc}\|}\left[\left(L_0 - L_1 cos2\tilde{\theta}\right) + \left(L_{dq} sin2\tilde{\theta}\right) + \left(-L_2\, cos\left(h_2\theta + 2\tilde{\theta}\right)\right)\right] sin\omega_{hf}t \quad (4\text{-}6)$$

$$i_{qc} = \frac{V_{hf}}{\omega_{hf}\|\mathbb{L}_{dqc}\|}\left[\left(-L_1 sin2\tilde{\theta}\right) + \left(-L_{dq} cos2\tilde{\theta}\right) + \left(-L_2\, sin\left(h_2\theta + 2\tilde{\theta}\right)\right)\right] sin\omega_{hf}t \quad (4\text{-}7)$$

Where

$$\|\mathbb{L}_{dqc}\| = L_0^2 - L_1^2 - L_2^2 - L_{dq}^2 - 2L_1 L_2\, cos(h_n\theta) - 2L_{dq} L_2 sin\,(h_n\theta) \quad (4\text{-}8)$$

4.2 Rotor Position and Speed Estimation of HFI Scheme

Different from estimation at zero-speed, low speed estimation is more challenging due to:

1. Fundamental excitation is introduced and high frequency signal becomes noisy
2. Different load level requires fast response of observer.

Figure 8 shows the block diagram of HFI-based observer for low speed operation. In the observer, both i_{dc} and i_{qc} are modulated to form rotor position error. Error reconstruction block reconstructs rotor position through knowledge of cross coupling or secondary salience, which are functions of fundamental stator current.

Figure 8. Block Diagram of HFI Observer at Low Speed

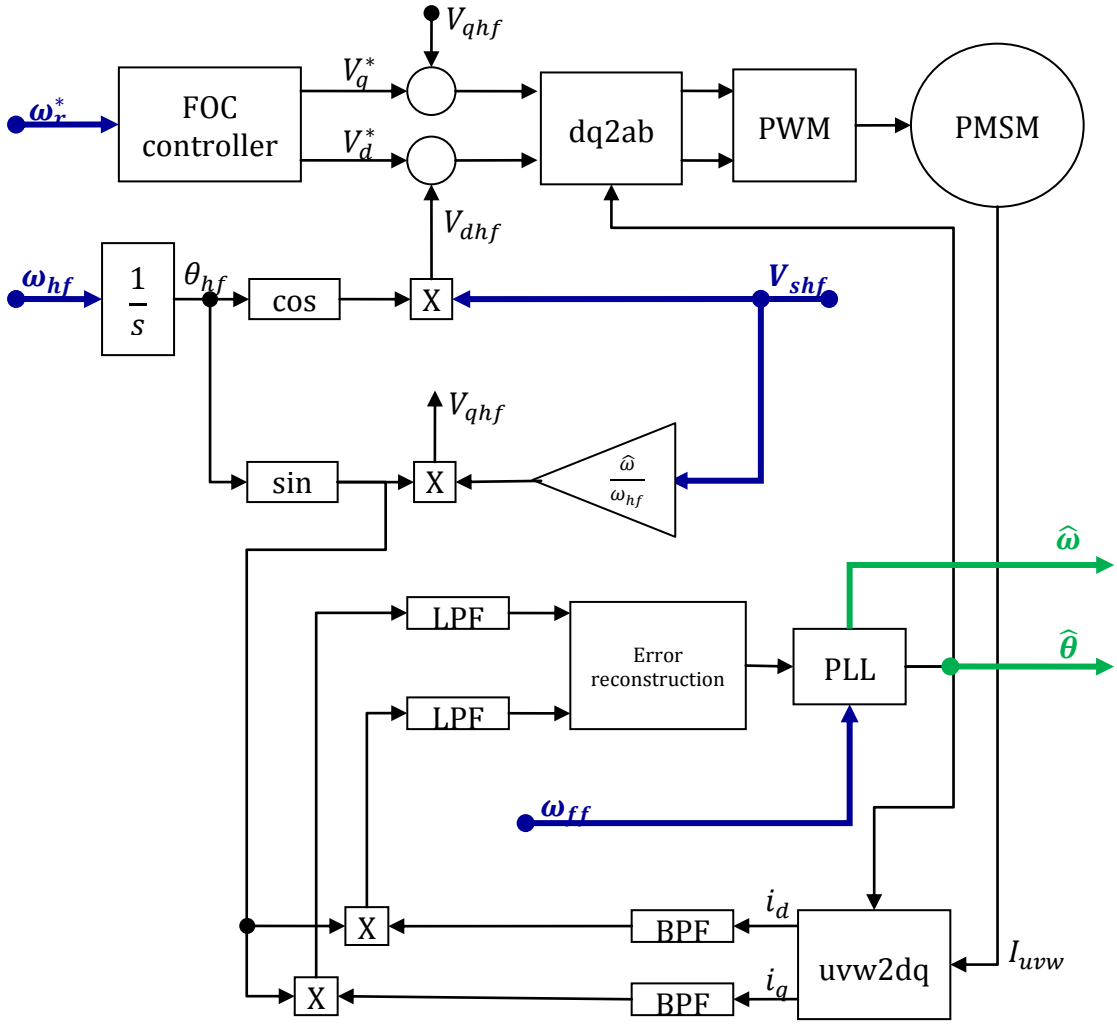

Figure 9. Block diagram of PLL at low speed

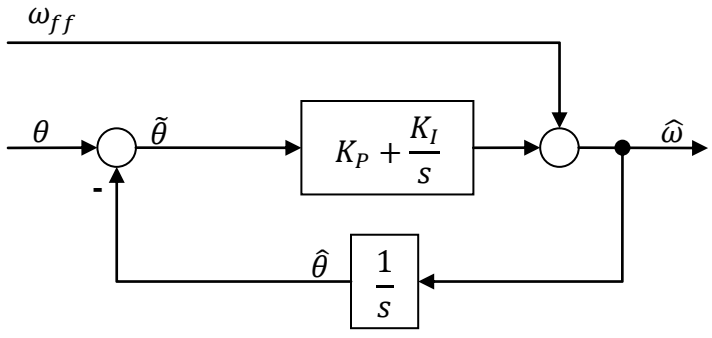

Figure 9 shows the block diagram of PLL for rotor speed and position estimation. Different from zero speed PLL, I-regulator is implemented for noise suppression and tracking capability promotion, and speed feed forward is added to extend its bandwidth.

5 Experiment Result

5.1 Initial Position Detection

The experiment is conducted on 4 types of motors. Zero speed HFI-based position estimation is first introduced to estimate rotor position, and polarity detection is followed to correct HFI estimation. Table 1 shows the specified parameters of each test motor

Table 1. Motor parameters

Motor	Pole pairs	R_s(Ohm)	L_d(mH)	L_q(mH)	λ_f(V_{rms}/krpm)
DA89	2	0.355	5.6	9.1	22
DA130	3	1.000	10.0	15.0	35
WM motor	2	1.500	18	20	-
Refrigerator	2	3.9	100.0	150.0	40

In below tests, each signal indicates:

1. Yellow: Motor phase current
2. Cyan: Estimated position error
3. Purple: Estimated rotor speed
4. Green: Estimated rotor position

5.1.1 DA89 Test

DA89 experiment is done in an AC system. Table 2 and Table 3 show the test condition and test result of DA89, and the statistical result is calculated from 40 estimations. Figure 10 shows the initial position detection of DA89, including zero speed HFI estimation and polarity detection.

Table 2. Test condition of DA89

f_{hf}(Hz)	$I_{hf}(A)$	Total Test	Total Fail
625	0.4	350	0

Table 3. Statistical result of DA89 test

Min($\hat{\theta}$)	Max($\hat{\theta}$)	Avg($\hat{\theta}$)
255	277	259

Figure 10. Initial Position Detection on DA89

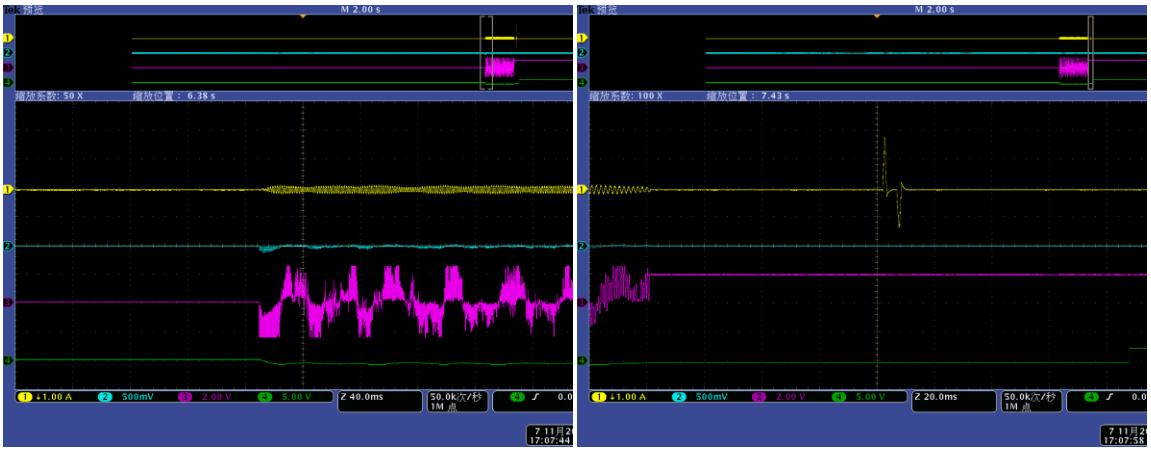

HFI estimation at zero speed Polarity detection

5.1.2 DA130 Test

DA130 experiment is done in an AC system. Table 4 and Table 5 show the test condition and test result of DA89, and the statistical result is calculated from 40 estimations. Figure 11 shows the initial position detection of DA130, including zero speed HFI estimation and polarity detection.

Table 4. Test condition of DA130

f_{hf}(Hz)	$I_{hf}(A)$	Total Test	Total Fail
625	0.4	350	0

Table 5. Statistical Result Of DA130 Test

Min($\hat{\theta}$)	Max($\hat{\theta}$)	Avg($\hat{\theta}$)
267	276	271

Figure 11. Initial position detection on DA130

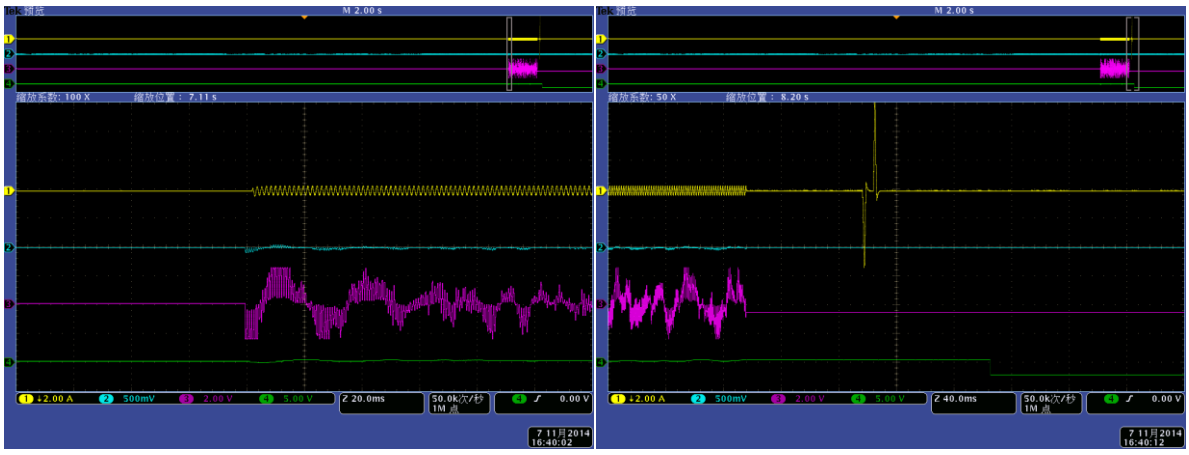

HFI estimation at zero speed Polarity detection

5.1.3 WM Motor Test

The washing machine motor is tested on a motor with tunable rotor position. Table 6 and Table 7 shows the test condition and test result of WM motor, each statistical result is calculated from 15 estimations. Because the WM is a 2 pole-pair motor, a total 360 mechanical angle is tested. Figure 12 shows the initial position detection of WM motor, including zero speed HFI estimation and polarity detection.

Table 6. Test Condition of WM Motor

f_{hf}(Hz)	$I_{hf}(A)$	Total Test	Total Fail
625	0.4	350	0

Table 7. Statistical Result of WM Motor Test

No.	Min($\hat{\theta}$)	Max($\hat{\theta}$)	Avg($\hat{\theta}$)
1	86	93	90
2	143	159	151
3	205	218	210
4	261	273	267
5	326	340	333
6	24	33	28
7	85	95	90
8	144	155	151
9	203	214	209
10	261	274	269
11	324	343	334
12	26	32	29

Figure 12. Initial Position Detection on WM Motor

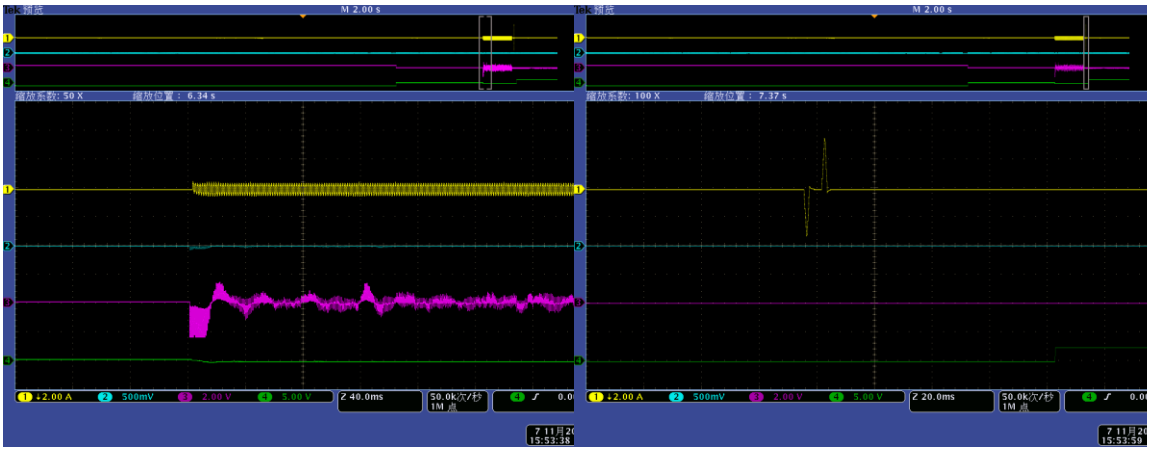

HFI estimation at zero speed

Polarity detection

5.1.4 Refrigerator Motor Test

Refrigerator experiment is done in a refrigerator system. Table 8 and Table 9 show the test condition and test result of refrigerator motor, and the statistical result is calculated from 40 estimations. Figure 13 shows the initial position detection of refrigerator motor, including zero speed HFI estimation and polarity detection, respectively.

Table 8. Test Condition of Refrigerator Motor

f_{hf}(Hz)	$I_{hf}(A)$	Total Test	Total Fail
625	0.4	350	0

Table 9. Statistical Result of Refrigerator Motor Test

Min($\hat{\theta}$)	Max($\hat{\theta}$)	Avg($\hat{\theta}$)
325	343	332

Figure 13. Initial Position Detection On Refrigerator

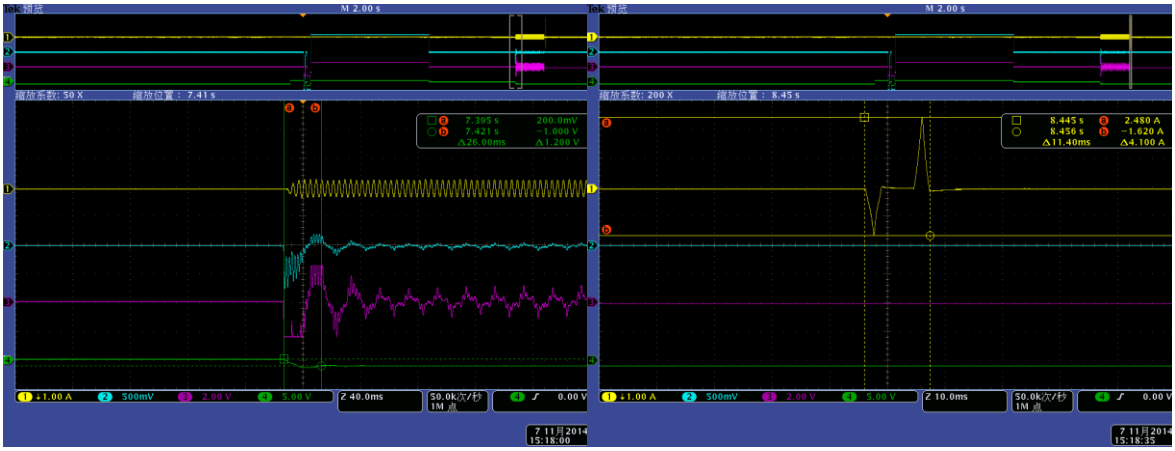

HFI estimation at zero speed　　Polarity detection

5.2 Low Speed FOC Drive

The low speed FOC drive tests the start-up process of motor, with different load conditions considered. In this experiment, 3 types of motors are tested.

In each test, start-up is fulfilled as below

1. Zero speed position estimation through HFI
2. Polarity detection
3. Low speed position estimation through HFI (with no fundamental current)
4. Low speed HFI observer-based FOC drive
5. EMF observer-based FOC drive

Particularly, when motor is driven to a certain speed, HFI observer is turned off, and high frequency voltage injection is stopped, too.

5.2.1 DA89 Test

DA89 motor test is done under light and heavy load conditions. Figure 14 shows the experiment with light load. Motor is started smoothly with HFI-based low speed observer, and position observer is switched into EMF observer at speed higher than 20 Hz (elec. speed).

Figure 15 shows the experiment result with heavy load. In this condition, HFI estimation has introduced harmonics, due to large fundamental current and nonlinear distortion of motor parameters.

Figure 14. Light Load Start-Up of DA89

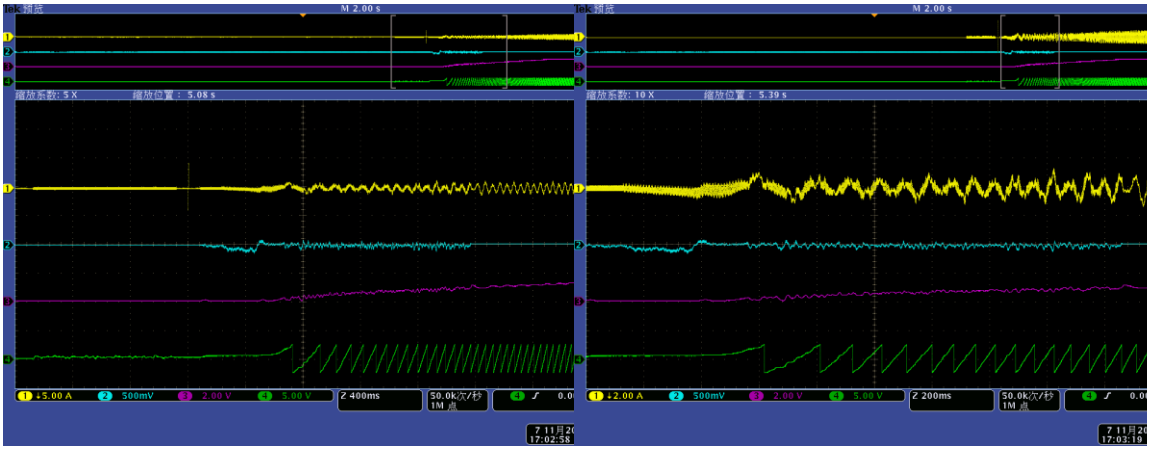

Figure 15. Heavy load start-up of DA89

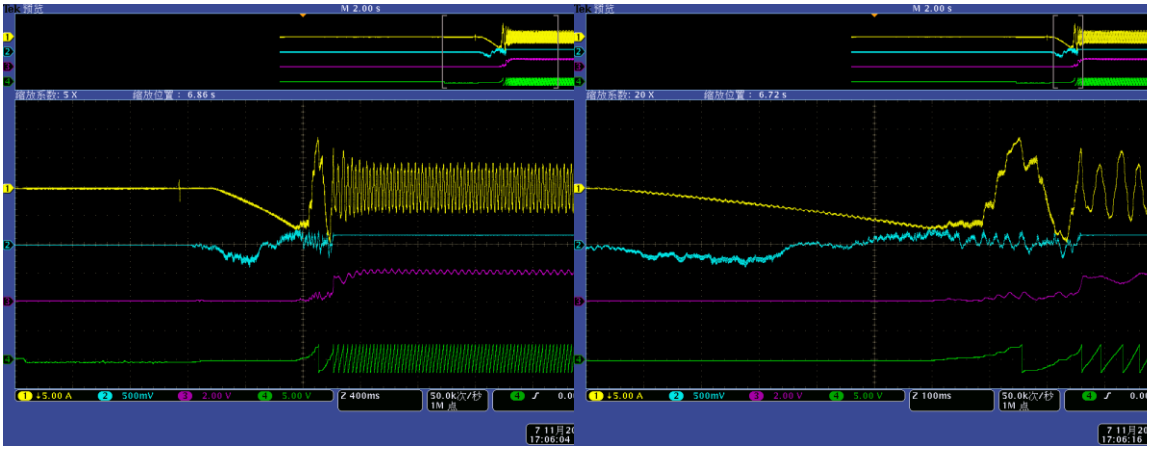

5.2.2 DA130 Test

DA130 motor test is done under light and heavy load condition. Figure 16 shows the experiment with light load. Motor is started smoothly with HFI-based low speed observer, and position observer is switched into EMF observer at speed higher than 20 Hz (elec. speed).

Figure 17 shows the experiment result with heavy load. In this condition, HFI estimation has introduced harmonics, due to large fundamental current and nonlinear distortion of motor parameters.

Figure 16. Light Load Start-Up of DA130

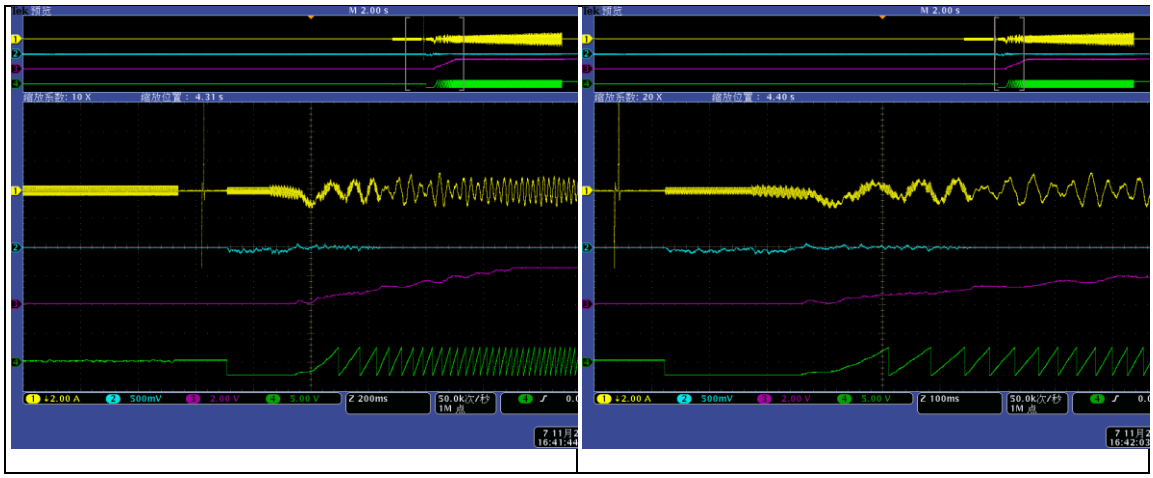

Figure 17. Heavy load start-up of DA130

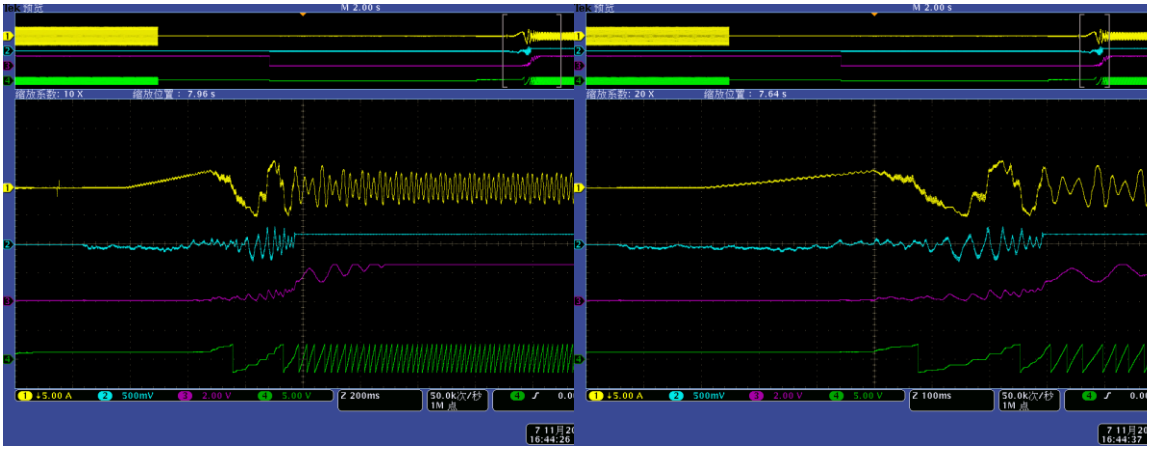

5.2.3 Refrigerator Test

Refrigerator motor test are done under light load condition. Figure 18 shows the experiment of this test.

Figure 18. Slight Load Start-Up of Refrigerator

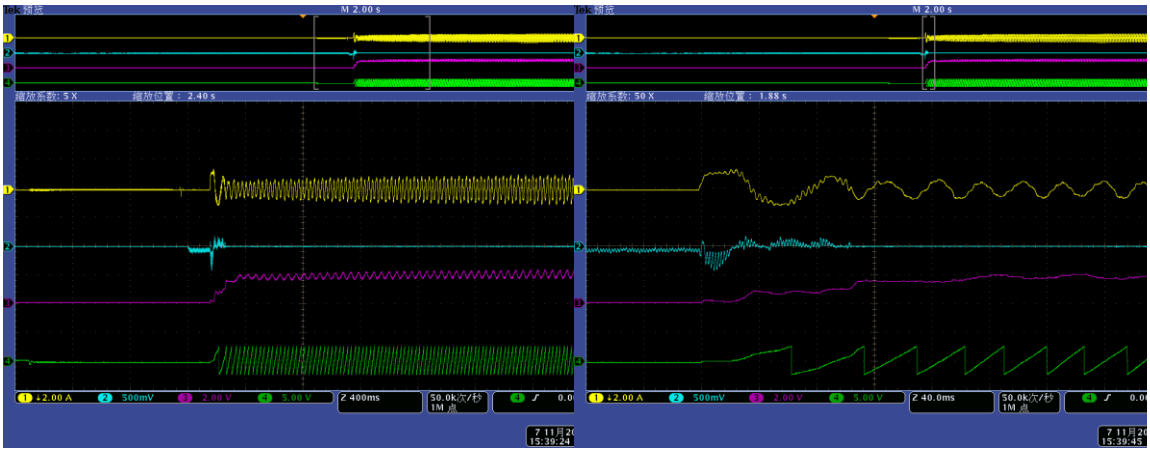

6 Document History

Document Title: AN204470 - FM3 Family, Position Estimation of PMSM with Signal Injection

Document Number: 002-04470

Revision	ECN	Orig. of Change	Submission Date	Description of Change
**	-	CBZH	06/26/2014	Initial release
*A	5100164	CBZH	01/22/2016	Migrated Spansion Application Note from MCU_AN709-00016-1v0-E to Cypress format
*B	5815392	AESATMP8	07/13/2017	Updated logo and Copyright.

Worldwide Sales and Design Support

Cypress maintains a worldwide network of offices, solution centers, manufacturer's representatives, and distributors. To find the office closest to you, visit us at Cypress Locations.

Products

ARM® Cortex® Microcontrollers	cypress.com/arm
Automotive	cypress.com/automotive
Clocks & Buffers	cypress.com/clocks
Interface	cypress.com/interface
Internet of Things	cypress.com/iot
Memory	cypress.com/memory
Microcontrollers	cypress.com/mcu
PSoC	cypress.com/psoc
Power Management ICs	cypress.com/pmic
Touch Sensing	cypress.com/touch
USB Controllers	cypress.com/usb
Wireless Connectivity	cypress.com/wireless

PSoC® Solutions

PSoC 1 | PSoC 3 | PSoC 4 | PSoC 5LP | PSoC 6

Cypress Developer Community

Forums | WICED IOT Forums | Projects | Videos | Blogs | Training | Components

Technical Support

cypress.com/support

Cypress Semiconductor
198 Champion Court
San Jose, CA 95134-1709